Available online at www.sciencedirect.com

ScienceDirect

Physics Procedia 83 (2016) 396 – 405

Physics Procedia

9th International Conference on Photonic Technologies - LANE 2016

High-power laser welding of thick steel-aluminum dissimilar joints

Rabi Lahdo[a,*], André Springer[a], Ronny Pfeifer[a], Stefan Kaierle[a], Ludger Overmeyer[a]

[a]*Laser Zentrum Hannover e.V., Hollerithallee 8, 30419 Hannover, Germany*

Abstract

According to the Intergovernmental Panel on Climate Change (IPCC), a worldwide reduction of CO_2-emissions is indispensable to avoid global warming. Besides the automotive sector, lightweight construction is also of high interest for the maritime industry in order to minimize CO_2-emissions. Using aluminum, the weight of ships can be reduced, ensuring lower fuel consumption. Therefore, hybrid joints of steel and aluminum are of great interest to the maritime industry.

In order to provide an efficient lap joining process, high-power laser welding of thick steel plates (S355, t = 5 mm) and aluminum plates (EN AW-6082, t = 8 mm) is investigated. As the weld seam quality greatly depends on the amount of intermetallic phases within the joint, optimized process parameters and control are crucial. Using high-power laser welding, a tensile strength of 10 kN was achieved. Based on metallographic analysis, hardness tests, and tensile tests the potential of this joining method is presented.

Peer-review under responsibility of the Bayerisches Laserzentrum GmbH

Keywords: high-power laser welding; steel-aluminum; dissimilar joints; lightweight construction; maritime industry

1. Motivation

For lightweight construction, steel-aluminum hybrid material combinations are of high interest, due to their properties regarding strength (steel) and density (aluminum). Such hybrid material combination can be used to minimize the weight of parts. Many steel-aluminum applications are already used in the manufacturing of car bodies (Brüdgam et al., 2004; Bayraktar et al. 2008; Assunção et al., 2010). Besides the automotive sector, lightweight construction is also of high interest for maritime industry to reduce the weight of ships and subsequently the CO_2-emissions. The consumption of fuel must be limited in order to fulfil requirements concerning CO_2-emissions (Waterborne Strategic Research Agenda, 2011; El Moctar, 2010). The Intergovernmental Panel on Climate Change

* Corresponding author. Tel.: +49-5112788-358 ; fax: +495112788-100 .
E-mail address: r.lahdo@lzh.de

Peer-review under responsibility of the Bayerisches Laserzentrum GmbH
doi:10.1016/j.phpro.2016.08.041

(IPCC) led in the Energy Efficiency Design Index (EEDI) for the global freight traffic. This regulation stipulates that new ships have to be 30% more efficient by 2025. The aim is a reduction of CO_2-emissions of up to 263 million tons (The International Council on Clean Transportation, 2011). Lightweight construction is also of high interest for yachts and military ships to lower the center of gravity of the ship and thus stabilize it enabling an increase of speed (Schiffbautechnische Gesellschaft, 2001). Thus, the yacht design employs ship hull of steel and deck constructions of aluminum alloys. To join both parts, an explosive welding adapter is applied, but the manufacturing of this adapter is complex, time-consuming and costly. These adapters have a oversized thickness, depending on the material thickness of the steel and aluminum alloys, in order to meet the required strength. Fig. 1 illustrates an explosive welded adapter (left) (Buijs, 2004) and an example of a steel-aluminum application in the ship sector (right) (FSW-Ship project, 2013).

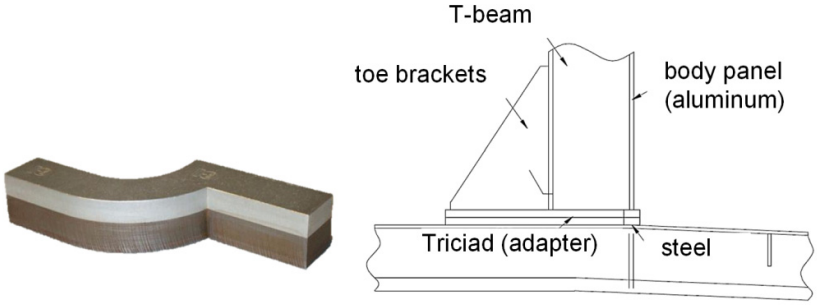

Fig. 1. Explosive welded adapter (left) (Buijs2004) and a typical application of steel-aluminum components in the ship sector (right) (FSW-Ship project, 2013).

The aim of the presented investigation is to develop a laser welding process in keyhole-modus for joining steel (S355, t = 5 mm) to aluminum (EN AW-6082, t = 8 mm) plates and to characterize the weld seam.

2. State of the art

2.1. Mechanical und chemical properties of formed intermetallic compounds

Thermal joining of steel and aluminum is associated with high challenges regarding material and process, due to the different physical properties of iron and aluminum (Klock et al., 1977). Especially, the different melting temperatures, thermal conductivity and thermal expansion lead to induced tension and distortion of the components. Aluminum and iron are almost unsoluble regarding each other in the solid state. Due to this low solubility, the formation of intermetallic compounds occurs, which are characterized by hard and brittle phases. As a result, the strength and the fatigue behavior of the weld seams is degraded, and premature failure of the weld seams occur (Steiners, 2011; Staubach, 2009, Radscheit, 1997). Depending on the aluminum content in the weld pool, various Fe_xAl_y structures, for example Fe_3Al (Al: 25 at.%), FeAl (Al: 50 at.%), $FeAl_3$,(Al: 74 - 76 at.%) and Fe_2Al_5 (Al: 69.7 - 73.2 at.%), are formed. Since the aluminum-rich intermetallic phases have a comparatively high hardness of about 1000 HV, they also have a low forming capacity and high susceptibility to cracking (Radscheit, 1997).

2.2. Steel-aluminum dissimilar joints

Mechanical and thermal joining technologies are used to join steel to aluminum. Clinching and riveting (Brüdgam et al., 2004; Simon, 2007), as mechanical joining technologies, are often combined with adhesive methods (Friedrich, 2013). Clinching or riveting are used for fixing the parts during the hardening of an adhesive based on epoxy. The brazing processes, for example arc brazing (Trommer, 2011), inductive brazing (Roulin et al., 1999) and laser brazing (Nothdurft el al., 2015) belong to the thermal joining technologies. To realize a brazing process for steel and aluminum, the steel has to be coated with zinc and the oxide layer on the aluminum surface

needs to be removed by using a flux. Sometimes a combination of brazing and welding is used, whereby the aluminum is molten and the steel remains in solid state (Aichele, 2008). These joining technologies are conventionally used to join dissimilar matarials with a thickness up to 2 mm. For ship building applications, thicker sheets up to 10 mm are required (FSW-Ship project, 2013). Dissimilar joints with a thickness of 3 mm can be joined in butt configuration, for example using laser-MIG hybrid joining (Thomy et al., 2007). Another kind of laser welding-brazing technique is used to join a 2 mm upper steel sheet with a 6 mm lower aluminum sheet in an overlap configuration. The laser heats up the steel so that the aluminum melts and wets the steel surface. In a shear tensile test, the weld seams achieve a max. shear force up to 30 kN, using a sample width of 60 mm (Meco et al., 2015). Additional standard joining technologies are friction welding and friction stir welding. These provide benefits regarding the creation of welded seams with a modest degree of brittleness due to a low amount of intermetallic phases (Kimapong et al., 2004; Merklein, 2011). The disadvantages of this welding procedure are high tool wear, due to the high process forces, and compared to other joining technologies, a low feed rate and long process duration. Friction stir welding can be used to join steel to aluminum with a maximum sheet thickness of 4 mm (FSW-Ship project, 2013). Explosive welding is used to join dissimilar materials for applications in the field of chemical apparatus, large engines and ship building. In this process, the dissimilar parts are joined by a shock wave resulting from an explosion (Tostman, 2001). The benefits of this procedure are non-porous seams with a low degree of mixing and a narrow heat effected zone. Because of the shock wave, the thicknesses of the cladding material is reduced, so that explosive welded seams have to be designed with a higher thickness (Heubner et al., 2009). The main disadvantage lies in the high costs of this special procedure.

For joining steel and aluminum, laser welding is the focus of many research investigations, in particular, for the automotive sector (sheet thickness of about 1 mm), due to its properties with respect to local heat input. For this, a lap joint configuration with steel on aluminum was applied, and within these investigations, the formation of intermetallic phases in the weld seams, depending on the molten aluminum, could be reduced by a limitation of the penetration depth. Using proper welding parameters, a high weld seam quality without macro-cracks, and a high shear force up to 5 kN could be achieved (Kaierle et al., 2014; Kallage, 2013; Sierra et al., 2007).

3. Experimental setup and materials used

The welding process was carried out using a solid-state laser Trumpf TruDisk 16.002, with a maximum laser power of 16 kW and high laser beam quality. Using a focal length of 300 mm and a line of collimation with a length of 200 mm, a spot diameter of 0.3 mm resulted. The one-sided welding process was developed for an overlap joint with steel as the upper sheet and aluminum as the lower sheet. For the welding investigations, a sample size of 120 x 200 mm (overlap: 40 mm) was used. The materials for the dissimilar joints were steel with grade of S355 (t = 5 mm) and an aluminum alloy EN AW-6082 (t = 8 mm). In table 1, the mechanical properties of the materials used are listed.

Table 1. Mechanical properties of the materials used.

Material	Yield strength [MPa]	Ultimate tensile strength [MPa]
S355 (t = 5 mm)	456	556
EN AW-6082 (t = 8 mm)	303	325

4. Evaluation procedure

For the development of the welding process, a defocused laser beam was used in order to realize different spot diameters, from 0.83 up to 1.90 mm. Table 2 shows the calculated intensity and the minimal energy per unit length needed to weld through the upper steel sheet using a constant laser power of 6 kW, depending on the spot diameter. To determine the influence of the energy per unit length on the properties of the weld seam, the weld speed was varied.

Table 2. Spot diameter, calculated intensity and minimal energy per unit length depending on coaxial focus position.

coaxial focus position [mm]	spot diameter [mm]	calculated intensity [W/cm²]	energy per unit length [kJ/m]
-5.0	0.83	1.11·106	85
-7.5	1.10	0.75·106	120
-10.0	1.37	0.41·106	200
-12.5	1.63	0.29·106	300
-15.0	1.90	0.21·106	600

The quality of the weld seams, regarding surface imperfections, was determined using visual inspection. For characterization of the weld seam geometry, meaning width and penetration depth as well as crack length in the weld-in area and metallurgy, cross-sections were taken. By using nital with a nitric acid concentration of 3%, the microstructure of the weld metal, the heat affected zone, the base material and intermetallic compounds can be made visible. Fig. 2 illustrates schematically the determination of the geometric variables, respectively the classification of the different measurement lines of the weld seam.

The shear tensile tests were carried out with a testing speed of 10 mm/min, using samples size with a width of 25 mm, a length of 200 mm and an overlap of 40 mm. Beside the maximal shear force, the type and the position of the fracture is documented.

The hardness test method based on Vickers was done according to DIN EN ISO 6507-1. The hardness profiles, using a test load of 1.96 N (HV0.2) across the base material, heat affected zone, weld metal and intermetallic phases were taken at different distances from the top, see line I (2.5 mm), line II (5 mm), line III (6.5 mm), line IV (8 mm) and line V (from top to bottom) in Fig. 2.

In order to establish a correlation between hardness and chemical composition at different measuring zones, EDX-line scans were performed using a scanning electron microscope (SEM).

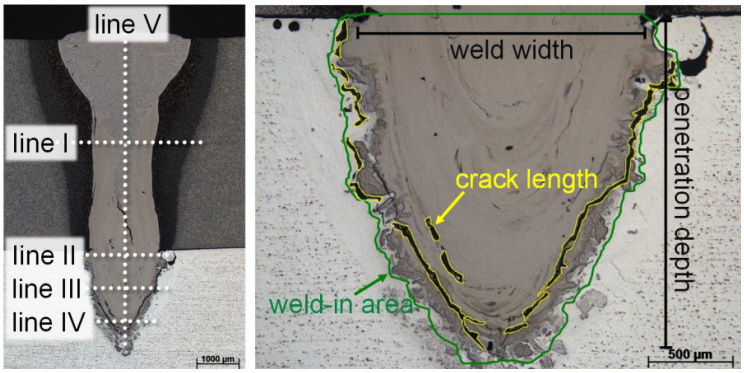

Fig. 2. Determination of geometric variables and measurment lines.

5. Results and discussion

5.1. Metallographic investigations

Within the context of this investigation, the influence of energy per unit length on the microstructure and the distribution of aluminum within the weld seam was determined in dependency of the used spot diameters of 0.83 mm and 1.63 mm. Several cross-sections are shown in Fig. 3.

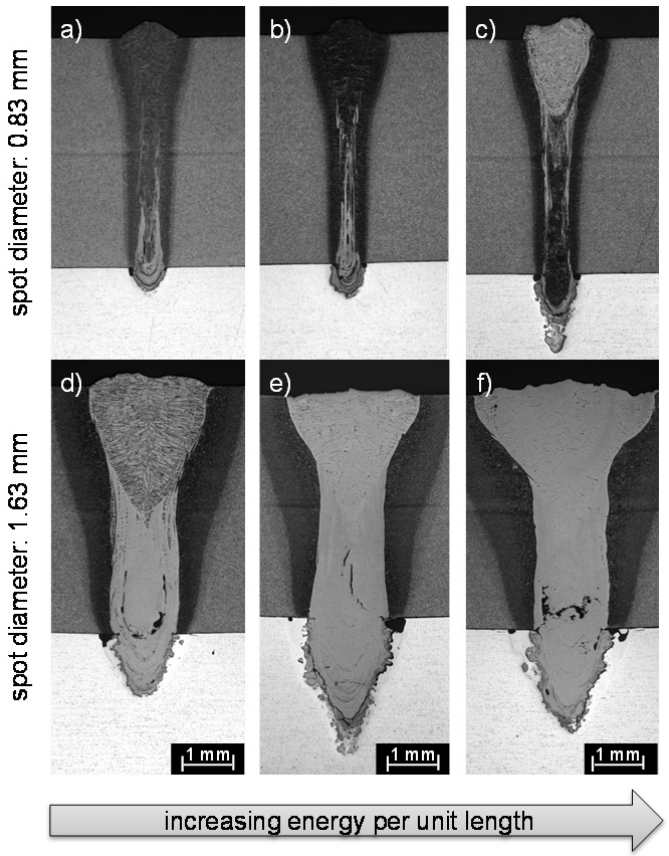

Fig. 3. Influence of various energy per unit length of 90 kJ/m (a), 95 kJ/m (b) und 115 kJ/m (c), using a spot diameter of 0.83 mm and energy per unit length of 300 kJ/m (d), 360 kJ/m (e) and 450 kJ/m (f), using a spot diameter of 1.63 mm on microstructure and distribution of aluminum within the weld seam.

The influence of the energy per unit length on the microstructure, and the distribution of aluminum for the lower spot diameter of 0.83 mm can be observed, based on the cross-sections (a - c). The aluminum content within the weld seam increases with higher energy per unit length, due to higher penetration depths and weld widths depending on melt flow. The aluminum is concentrated to form the phases Fe_3Al (Al: 25 at.%), FeAl (Al: 35 at.%) and iron solid solution (up to Al: 20 at.%) at the top and on the side of the weld seam. The aluminum content at the top decreases with higher energy per unit length. Using energy per unit length of 95 kJ/m (b), no aluminum is detected at the top of the weld seam. The aluminum content accumulates in the weld-in area to the middle of the weld seam. Accumulation decreases when using higher energy per unit length. By using a low energy per unit length of 90 kJ/m (a), the molten aluminum mostly remains in the weld-in area, and on the side of the weld seam. But for all cross-sections, a part of the weld is characterized by bainitic and martensitic structures. In these areas, the aluminum content is not high enough to transform the microstructure to an iron solid solution. The amount of the bainitic and martensitic structures increases for a decreasing energy per unit length.

With respect to a spot diameter of 1.63 mm, also different microstructures, depending on the energy per unit length, can be observed. An increasing energy per unit length leads to a higher aluminum content in the weld seam, and the microstructure does not include bainitic and martensitic structures. At the top of the weld seam, an aluminum content of 7 at.% (using an energy per unit length of 300 kJ/m (d)), of 11 at.% (using an energy per unit length of 360 kJ/m (e)) and of 14 at.% (using an energy per unit length of 450 kJ/m (f)) can be detected. Depending on the aluminum content, an iron solid solution and Fe_3Al-phases are formed. Furthermore, the aluminum content

increases from the top of the weld seam (Al: 11 at.% (e)) to the weld-in area (Al: 35 at.% (e)), using an energy per unit length of 360 kJ/m. The aluminum-rich intermetallic phases like $FeAl_3$ or Fe_2Al_5 can be primary detected in weld-in area. Moreover a larger heat affected zone, penetration depth and weld width, independent of the spot diameter, can be observed. These cross-sections of the laser weld seams exhibit cracks within the weld center, and in particular in the transition zone from the molten pool to the aluminum alloy. A detailed determination of cracks regarding crack length within the weld-in area can be found in the next chapter.

5.2. Detection of cracks dependent on penetration depth and weld width

Cross-sections were taken to qualify the weld seam regarding cracks in the weld-in area and to determine the weld geometry. Fig. 4 shows the results concerning the penetration depth, weld width and crack length, depending on the energy per unit length and spot diameter of 0.83 mm (a), 1.1 mm (b), 1.63 mm (c) and 1.9 mm (d). For all weld seams, increased penetration depths and weld widths are related to increasing energy per unit length, but both varied strongly over the weld seam length. Moreover, the crack length also tendentially increases with higher penetration depths and weld widths, due to increased energy per unit length. Depending on the spot diameter and energy per unit length used, a relatively low crack length of 1560 µm (spot diameter of 0.83 mm and energy per unit length of 95 kJ/m (a)), 820 µm (spot diameter of 1.37 mm and energy per unit length of 200 kJ/m (b)), 3180 µm (spot diameter of 1.63 mm and energy per unit length of 300 kJ/m (c)) and 2500 µm (spot diameter of 1.90 mm and energy per unit length of 600 kJ/m (d)) are detected. The diagrams show that the penetration depth increases more, as compared to the weld width.

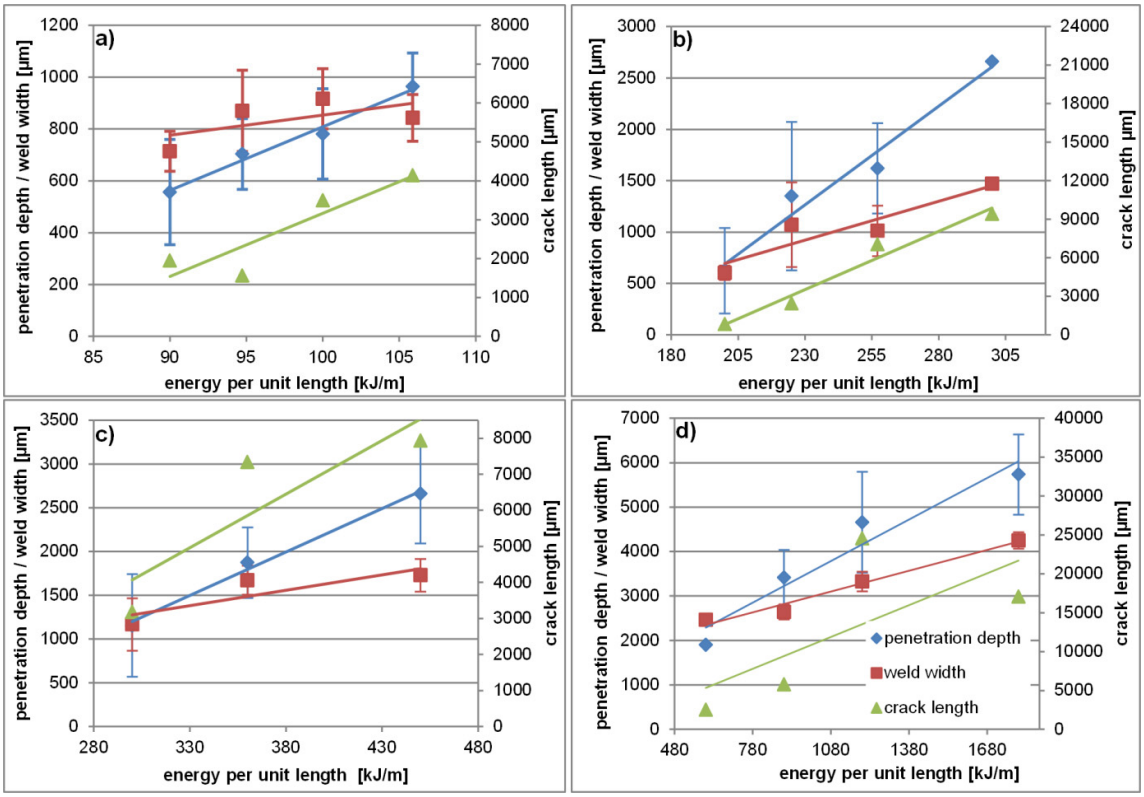

Fig. 4. Penetration depth, weld width and percentage of cracks, depending on the spot diameter of 0.83 mm (a), 1.37 mm (b), 1.63 mm (c) and 1.90 mm (d).

5.3. Shear tensile test

Within the context of these investigations, the results of shear tensile tests are shown in Fig. 5, depending on the energy per unit length and spot diameter of 0.83 mm (a) and 1.63 mm (b). Furthermore the maximum shear forces are determined concidering spot diameter and appropriate energy per unit length, see (a) in Fig. 6. The influence of increased weld width at a constant penetration depth on the shear force, depending on the energy per unit length, is presented in Fig. 6 (b).

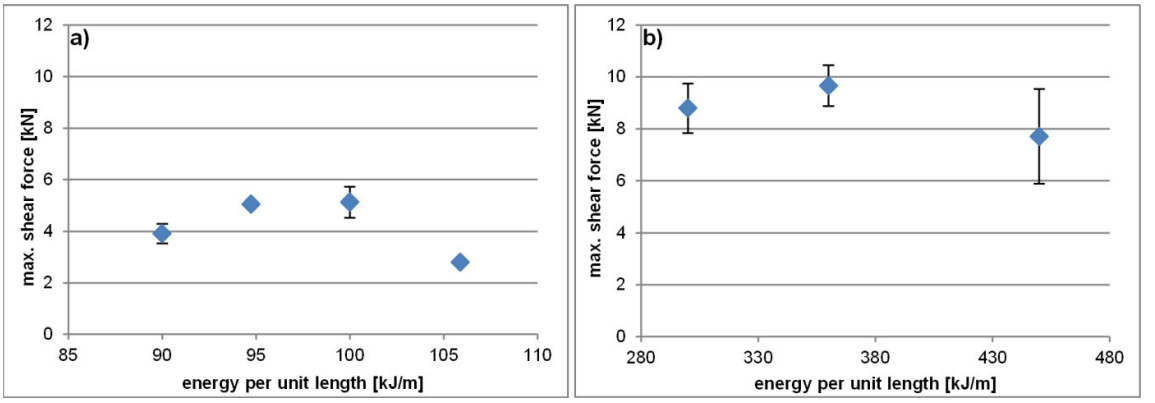

Fig. 5. Maximum shear force depending on the energy per unit length and spot diameter of 0.83 mm (a) and 1.63 mm (b).

The curve characteristics of the shear tensile force is approximately similar for all test series. First, the force increases for higher energy per unit length to a maximum force, and afterwards the force decreases, see Fig. 5 (a) and (b). It is possible to achieve a maximum shear force of 9.7 kN (this value corresponds to 16% of yield strength of EN AW-6082 and 32% of yield strength of EN AW-5083), using an energy per unit length of 360 kJ/m and spot diameter of 1.63 mm.

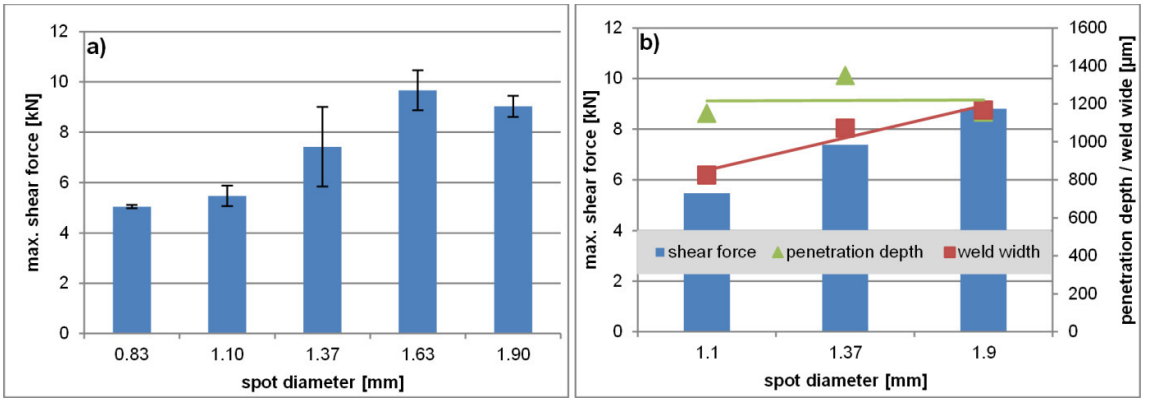

Fig. 6. Maximum shear force depending on the spot diameter at adapted energy per unit length (a) and maximum shear force depending on the weld width at constant penetration depth under considering of adapted energy per unit length (b).

Fig. 6 (a) illustrates the maximum achievable shear forces, depending on spot diameter and considering the adapted energy per unit length. An increased force is achieved with an increasing spot diameter up to 1.63 mm. Afterwards the force decreases. Using a spot diameter of 1.63 mm and 1.90 mm, the samples fail in the weld metal of the steel side, and by using a spot diameter of 0.83 mm, 1.10 mm and 1.36 mm, shear fracture occurs on the

samples. These results of the static shear tensile tests do not reflect the results concerning the crack length, due to the fact that shear force is affected by the weld geometry regarding the weld width, too. This only applies if the cracks are oriented parallel to the weld width. Fig. 6 (b) confirms that the shear force increases tendentially with an increasing weld width at constant penetration depth and under consideration of energy per unit length.

5.4. Results of scanning electron microscope and hardness tests

To determine the chemical composition, EDX-line scans (see Fig. 7) using a scanning electron microscope, are carried out on the samples welded with a spot diameter of 1.63 mm and an energy per unit length of 360 kJ/m (achievable highest shear forces). The line scans were taken transversely and longitudinally to the cross-section.

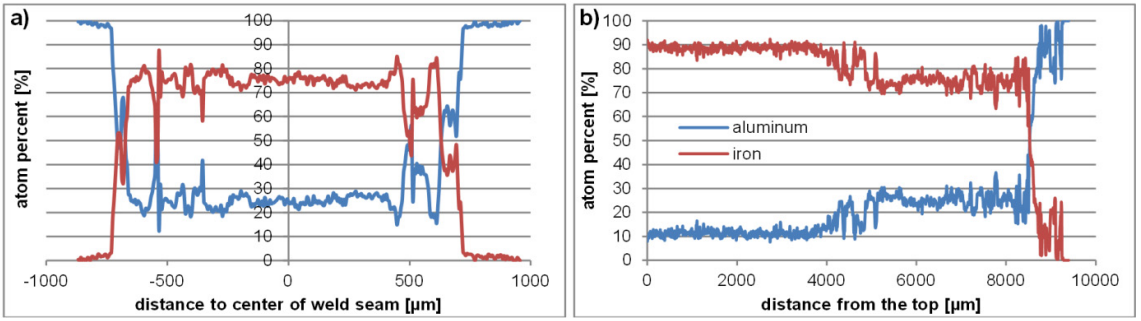

Fig. 7. EDX-line scans (line IV) transverse (a) and longitudinal (b) to the cross-section welded with a spot diameter of 1.63 mm and an energy per unit length of 360 kJ/m.

Additional, SEM images were taken, in particular, of the zone, where the cracks proceed in the weld-in area (see Fig. 8).

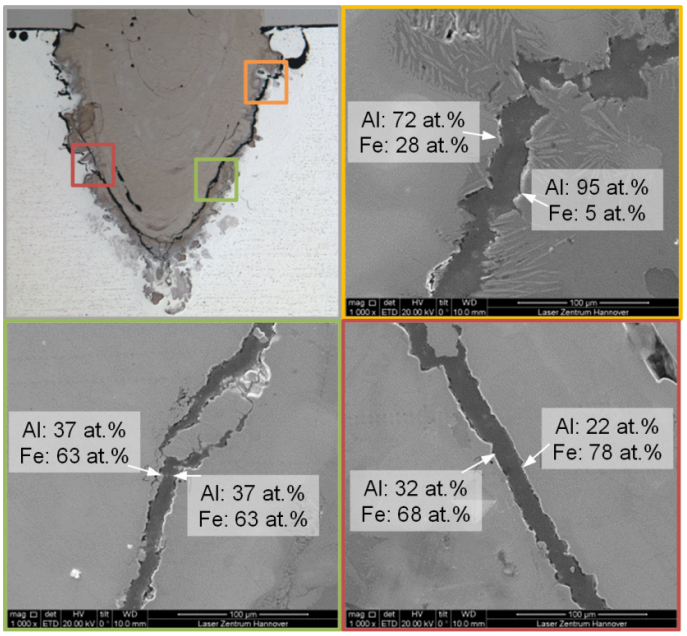

Fig. 8. Cross-section of weld-in area and SEM-Images with chemical analyses in the zones of the fracture.

Based on these results, it was shown that the cracks proceed through different microstructures like iron solid solution, base material of the aluminum alloy and intermetallic phases such as Fe_3Al, FeAl, Fe_2Al_5 and $FeAl_3$.

To determine a correlation between the chemical composition and the hardness, hardness profiles were carried out on the seam welded with a spot diameter of 1.63 mm and energy per unit length of 360 kJ/m. The steel base material has a hardness of 200 HV0.2, and the aluminum alloy EN AW-6082 of 85 HV0.2. Due to the heat treatment during welding, the hardness in the heat affected zone increases to 330 HV0.2 (see line I in Fig. 9). Based on the results of the longitudinal line scan, the aluminum content increases form 11 at.% to 17 at.% at a depth of 4 mm. In this measurement zone, a hardness range of 244 to 300 HV0.2 (average hardness of 270 HV0.2) results. In a measurement range from 4 mm to 5.5 mm, the hardness increases from 260 to 360 HV0.2 (with increasing aluminum content up to 25 at.%). Up to a penetration depth of 5.5 mm, the hardness varies from 300 to 366 HV0.2, which corresponds to an aluminum content of 20 to 35 at.%. These results, regarding the hardness of the weld metal, reflect the results of the transverse hardness profile, see line IV and V in Fig. 9. At a penetration depth of 6 mm (line V), a hardness of 500 to 600 HV0.2 of the aluminum-rich intermetallic phases can be detected. Due to the dimension of the intermetallic phases, the hardness cannot be precisely determined using a hardness method according to Vickers.

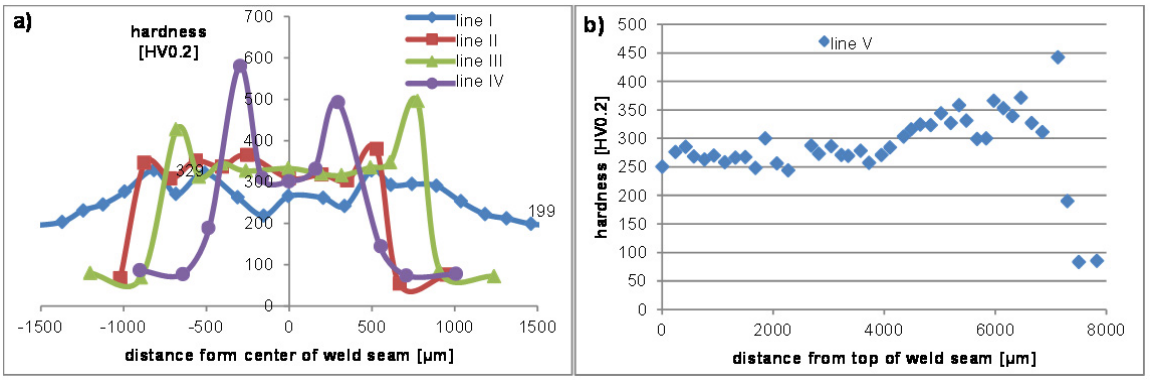

Fig. 9. Transver hardness profiles at different penetration depth (line I to V) (a) and longitudinal hardness profile (b) of the weld seam.

6. Conclusions

In these investigations, steel-aluminum dissimilar joints consisting of a steel plate S355 (t = 5 mm) and an aluminum plate 6082 (t = 8 mm) in overlap configuration were welded, using a high-power laser welding process. The weld seams were investigated using metallographic analysis to determine the weld geometry, the microstructure and the crack length. SEM was used to determine the chemical composition, while hardness tests and shear tensile tests characterize the mechanical properties. The metallographic investigations show that the penetration depth and weld width, depending on the spot diameter and energy per unit length, influence the microstructure and the appearance of cracks. The penetration depth, weld width and the crack length increase with higher energy per unit length. In a shear tensile test, the highest shear force of 9.7 kN was achieved, using a spot diameter of 1.63 mm and an energy per unit length of 360 kJ/m. The failure was located in the weld metal on the steel-side. These samples exhibit a higher crack length compared to the weld seam, which was welded with lower energy per unit length of 300 kJ/m. This means that the shear tensile force is affected by the weld width, too. Furthermore, the hardness corresponds to aluminum content in measurable microstructures. Due to the dimension of the intermetallic phases, the hardness cannot be precisely determined using a hardness method according to Vickers. Therefore a nano hardness tester would be suitable to measure the hardness of these phases.

Acknowledgements

The joint project “Laser Welding of Steel to Aluminum for Applications in Shipbuilding” (LaSAAS) is funded by the German Federal Ministry for Economics and Energy (BMWi), and supervised by the Forschungszentrum Jülich GmbH (PTJ). Furthermore, the authors wish to thank the project partners and the project committee member companies as well as their representatives for supporting the project and for their good cooperation.

References

Aichele, G., 2008. Verschweißen von Aluminum mit Stahl - Jedes der beiden Metalle zeigt sich von seiner besten Seite, in “*Industriebedarf*“ pp. 5-6, 14-16.

Assunção, E., Quintino, L., Miranda, R., 2010. Comparative study of laser welding in tailor blanks for the automotive industry, Int J Adv Manuf Technol 49, 123-131.

Schiffbautechnische Gesellschaft, 2001. 100 Jahre Schiffbautechnische Gesellschaft: Festveranstaltung vom 25. Bis 29. Mai 1999 in Berlin.

Bayraktar, E., Kaplan, D., Yilbas, B.S., 2008. Comparative study: Mechanical and metallurgical aspect of tailored welded blanks (TWBs), Jounal of Materials Processing Technology, 204, pp 440-450.

Brüdgam, S., Freitag, V., Hahn, O., Ruther, M., 2004. Optimization of joining techniques for multi-material constructions in body making.. ATZ worldwide 106 (12), pp. 23-27.

Buijs K., 2004. Triplate: The ultimate solution for welding aluminum to steel, HSB international.

El Moctar B., 2010. Ergebnisse der Arbeitsgruppe Schifffahrt, in “Symposium Schifffahrt und Meerestechnik für das 21. Jahrhundert“, Berlin.

Friedrich, H. E, 2013. Leichtbau in der Fahrzeugtechnik, Springer Vieweg, Wiesbaden.

Heubner, U., Klöwer, J., 2009. Nickelwerkstoffe und hochlegierte Sonderstähle: Eigenschaften - Verarbeitung – Anwendungen, Expert-Verlag Gmbh, pp 157-158.

The International Council on Clean Transportation, 2011. The Energy Efficiency Design Index (EEDI) for New Ships, public of The International Council on Clean Transportation.

Kimapong, K., Watanabe, T., 2004. Friction stir welding of aluminum alloy to steel, Welding Journal 10, pp. 277-282.

Kaierle, S., Pfeifer, R., Seffer, O., Schimek, M., Bös, J., Bolchoun, A.. 2014. Laserstrahlschweißen von Stahl an Aluminium mittels spektroskopischer Kontrolle der Einschweißtiefe und erhöhter Anbindungsbreite durch zweidimensional ausgeprägte Schweißnähte. Schlussbericht 2014, Forschungsvereinigung Automobiltechnik (FAT), FAT-Schriftenreihe 263.

Kallage, P., 2013. Laserschweißen von Mischverbindungen aus Aluminium und verzinktem sowie unverzinktem Stahl, Dissertation, Gottfried Wilhelm Leibniz Universität Hannover.

Klock, H., Schoer, H., 1977. Schweißen und Löten von Aluminiumwerkstoffen, Deutscher Verlag für Schweißtechnik, Düsseldorf.

Meco, S., Pardal, G., Ganguly, S., Williams, N., McPherson, N. 2015, Application of laser in seam welding of dissimilar steel to aluminum joints for thick structural components, Optics and Lasers in Engineering 67, pp. 22-30.

Merklein, M.. 2011. Innenhochdruck-Umformen reibrührgeschweißter Hybridstrukturen aus Stahl und Aluminium, DFG Projekt an der Friedrich-Alexander-Universität Erlangen-Nürnberg.

Nothdurft, S., Springer, A., Kaierle, S., Ross, J., Stonis, M., 2016. Laser soldering and brazing of steel-aluminum sheets for tailored hybrid tubes, Journal of Laser Applications, Volume 28, Number 2.

Radscheit, C., 1997. Laserstrahlfügen von Aluminium mit Stahl, Dissertation Universität Bremen, BIAS Verlag Bremen.

Sierra, G., Peyre, P., Deschaux-Beaume, F., Stuart, D., Fras, G., 2007. Steel to aluminium key-hole laser welding, Materials Science and Engineering A 447, pp. 197-208.

FSW-Ship project: final report: Rührreibgeschweißte Leichtbaustrukturen für Schiffsaufbauten, Abeking & Rasmussen Schiffs- und Yachtwerft Aktiengesellschaft; 2013.

Roulin, M, Luster, J. W., Karadeniz, G., Mortensen, A. 1999. Strength and Structure of Furnace-Brazed Joints between Aluminum and Stainless Steel, Welding Research Supplement, pp. 151-155.

Simon, S., 2007. Werkstoffgerechtes Konstruieren und Gestalten mit metallischen Werkstoffen, Habilitation Universität Cottbus.

Staubach, M., 2009. Eigenschaften schweißgelöteter Stahl-Aluminium-Mischverbindungen unter Verwendung wärmearmer MSG-Prozesse, Technische Universität Dresdem, Dissertation.

Steiners, Marius P., 2011. Lichtbogenfügen von beschichteten Stahlblechen an Aluminiumlegierungen, Rheinisch-Westfälische Technische Hochschule Aachen, Dissertation.

Thomy, C., Wagner, F., Vollertsen, F., Wirth, A., Kreimeyer, M., 2007. Laser-MIG-Hybrid-fügen von Aluminium-Stahl Leichtbaustrukturen. Laser Technik Journal 4, pp. 36-40.

Tostman, K.H., 2001. Korrosion. Ursachen und Vermeidung. Wiley-VCH (2001), pp. 206-207.

Trommer, G., 2011. Wann Löten lohnt. in “Konstruktion & Engineering 2“, pp. 42–44.

Waterborne Strategic Research Agenda, 2011. Waterborne Transport & Operations – Key for Europe’s Development and Future, European Technology Platform Waterborne, http://www.waterborne-tp.org, May 2011.